ACS Sustainable Chemistry & Engineering

Letter

Cite This: ACS Sustainable Chem. Eng. 2018, 6, 93−98

pubs.acs.org/journal/ascecg

Web-like 3D Architecture of Pt Nanowires and Sulfur-Doped Carbon Nanotube with Superior Electrocatalytic Performance

Md Ariful Hoque,[†,+] Fathy M. Hassan,[†,+] Altamash M. Jauhar,[†] Gaopeng Jiang,[†] Mark Pritzker,[†] Ja-Yeon Choi,[†] Shanna Knights,[‡] Siyu Ye,[‡] and Zhongwei Chen*[,†]

[†]Department of Chemical Engineering, Waterloo Institute for Nanotechnology, University of Waterloo, 200 University Avenue West, Waterloo, Ontario N2L 3G1, Canada

[‡]Ballard Power Systems Inc., 9000 Glenlyon Parkway, Burnaby, British Columbia V5J 5J8, Canada

Supporting Information

ABSTRACT: Development of highly durable electrocatalysts for oxygen reduction reaction (ORR) is critical for proton exchange membrane fuel cells. Herein, we report the synthesis, characterization, and electrochemical performance of 1D sulfur-doped carbon nanotubes (S-CNT) supported 1D Pt nanowires (PtNW/S-CNT). PtNW/S-CNT synthesized by a modified solvothermal method possesses a unique web-like 3D architecture that is beneficial for oxygen reduction. We demonstrate that PtNW/S-CNT exhibits impressive activity retention under potential cycling between 0.05 and 1.5 V vs RHE over 3000 cycles. The reductions in electrochemically active surface area (ECSA, 7% loss) and mass activity (19% loss) of PtNW/S-CNT after accelerated durability testing (ADT) are found to be much lower than the dramatic losses observed with commercial Pt/C (>99% loss in ECSA and mass activity) under identical conditions. The PtNW/S-CNT catalyst also shows very high specific activity (1.61 mA cm^{-2}) in comparison to Pt/C (0.24 mA cm^{-2}).

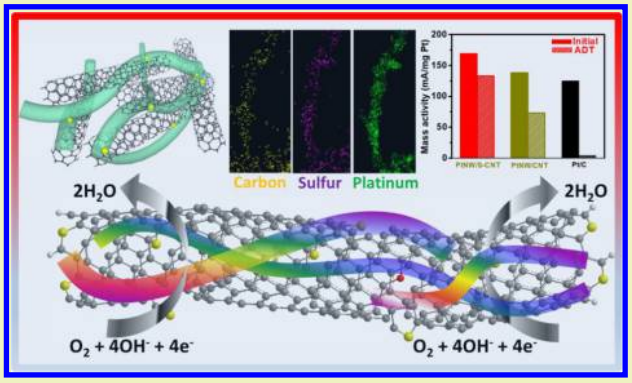

KEYWORDS: *Carbon nanotubes, Pt nanowires, Electrocatalyst, Oxygen reduction reaction, Fuel cells*

INTRODUCTION

The long enduring issue of durability of the platinum catalyst at the cathode is one of the most critical challenges that have restricted the widespread application of proton exchange membrane fuel cells (PEMFCs).[1] Catalysts undergo degradation during fuel cell operation due to aggregation, dissolution, and Ostwald ripening with carbon support corrosion, all of which cause a drop in electrochemical surface area (ECSA). These factors are responsible for the rapid drop in the power output of fuel cells.[2] Up until now, in commercial platinum catalysts, Pt nanoparticles of 2−5 nm dispersed on carbon black supports (Pt/C) have been the most widely used catalysts for the cathode.[3] However, these nanoparticles undergo an acute Ostwald ripening and/or grain growth due to the high surface energy associated with zero-dimensional (0D) nanostructured materials.[4−6] In addition, carbon black undergoes electrochemical corrosion at low potentials, leading to Pt nanoparticle migration, agglomeration, and detachment from the catalyst structure.[7]

The control of Pt nanostructures is one of the most effective directions for improving the durability of Pt-based catalysts against loss in ECSA.[4,8−10] For example, one-dimensional (1D) Pt nanostructures such as nanowires enjoy unique anatomical characteristics compared to their 0D counterparts, such as fast electron transfer; preferred orientation allowing exposure of highly active crystal facets; and high structural stability.[5,11] The structural anisotropy of nanowires has unique characteristic of slowing down the ripening process and impeding dissolution/aggregation, thereby improving catalytic durability and/or activity.[12] However, Pt nanowire catalysts grown onto stable supports such as carbon nanospheres (CNSs), carbon nanotubes (CNTs), and graphene have shown significant improvement in durability.[13−15] Among these support materials, CNTs possess outstanding properties such as high surface area, large electrical conductivity, great tensile strength, and excellent mass transport.[16] Doping of CNTs with heteroatoms has been practiced and reported as an efficient way to tune their intrinsic properties and improve electrocatalyst activity and durability.[17,18] We have previously established that sulfur-doped graphene (SG) has shown tremendous potential as a support material for Pt nanostructures and significantly improves stability in contrast with state-of-the-art Pt/C.[15,19] However, to our knowledge, the use of CNTs doped with sulfur (S-CNT) as Pt supports has not been reported in literature. We have

Received: October 5, 2017
Revised: November 6, 2017
Published: December 6, 2017

© 2017 American Chemical Society

DOI: 10.1021/acssuschemeng.7b03580
ACS Sustainable Chem. Eng. 2018, 6, 93−98

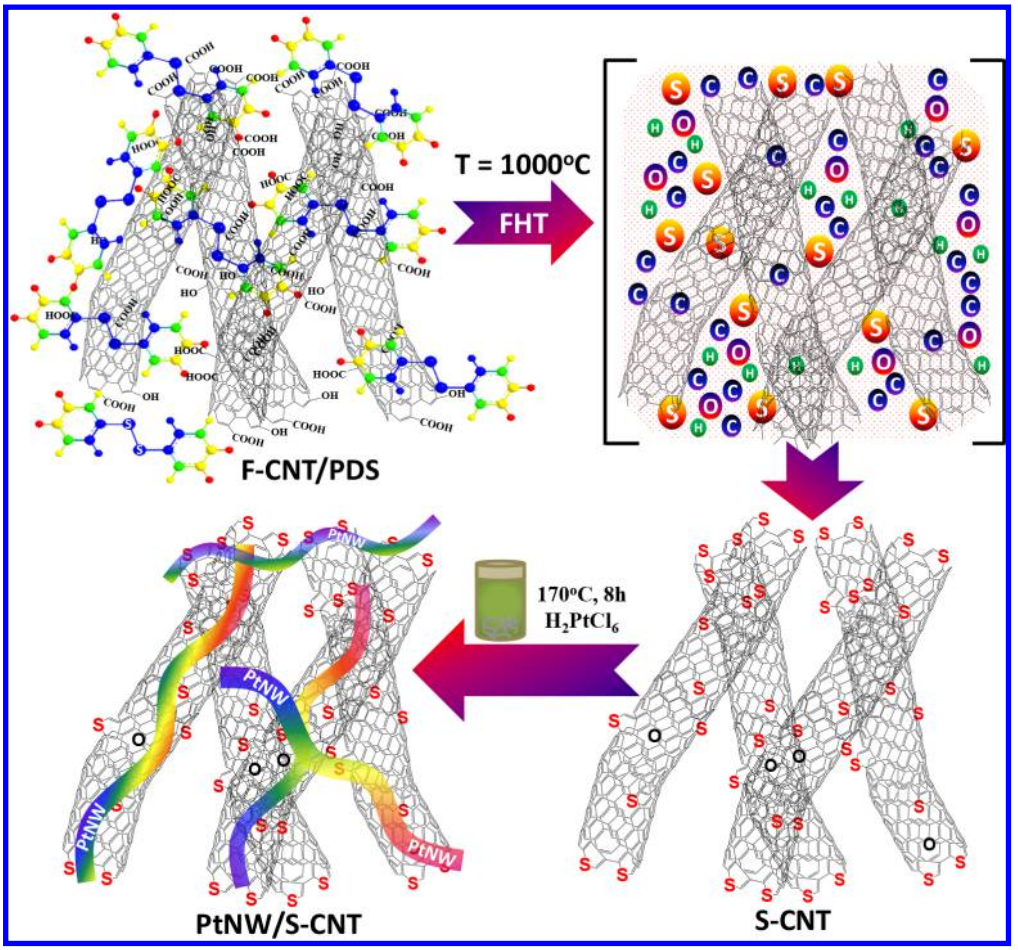

Figure 1. Schematic of the materials produced at different stages of S-CNT and PtNW/S-CNT synthesis.

successfully synthesized S-CNT to support Pt nanowire electrocatalysts for ORR and have shown that the newly developed material has incredible durability in harsh potentiodynamic conditions and the potential to have a significant impact in a wide range of applications.

Herein, we report an advanced and robust 3D electrocatalyst that addresses both the activity and durability problems associated with using 1D S-CNT-supported Pt nanowires (PtNW/S-CNT). We provide details concerning the structure, properties, and characteristics of S-CNT. We investigate and optimize the role of precursor materials on the formation of Pt nanowires on S-CNT. Our electrochemical study shows that PtNW/S-CNT exhibits exceptional activity retention over 3000 accelerated durability test (ADT) cycles over the potential range of 0.05 to 1.5 V vs RHE. The unique 3D features of PtNW/S-CNT will have a significant role in the promotion of future cathode electrocatalysts for practical applications.

RESULTS AND DISCUSSION

Figure 1 illustrates the flash heat treatment (FHT) process of as-prepared S-CNT and solvothermal synthesis of Pt nanowires on S-CNT. More details on the experimental procedure is provided in the Supporting Information. Briefly, the FHT process involves mixing F-CNT (functionalized CNT) with phenyl disulfide (PDS) and heating the solid mixture at high temperature (1000 °C). At this temperature, PDS decomposes to form carbonaceous gases and sulfur-free radicals, leading to the incorporation of sulfur atoms in the carbon framework of F-CNT. To grow and support the Pt nanowires onto S-CNT, we followed a simple solvothermal procedure without surfactant, which avoids any potential harmful effects of surfactant on the catalytic activity.

Figure 2a presents transmission electron microscopy (TEM) images of F-CNT collected at low magnification. F-CNTs have diameters of 25 ± 8 nm and can be as long as several micrometers. An energy dispersive spectroscopy (EDS) elemental map of carbon and oxygen in F-CNT (Figure 2b) reveals that functionalized oxygen groups have been integrated into the CNTs by contact with a HNO_3/H_2SO_4 mixture. High resolution TEM (HR-TEM) was used to count the number of walls in F-CNT, estimate the inner and outer diameters, investigate structural property, and identify anatomical changes (e.g., sidewall damages) induced due to surface modification.[20] The F-CNT in Figure 2c has a 6.2 nm inner diameter, 14.7 nm outer diameter, and consists of approximately 20 layers. The HR-TEM image of S-CNT in Figure 2d clearly indicates that the incorporation of S species by FHT does not alter the structural integrity of F-CNT. EDS mapping of carbon and sulfur in S-CNT (Figure 2e) shows that sulfur species are homogeneously distributed over the carbon network in the CNT. In conjunction with TEM, electron energy loss spectroscopy (EELS) can generate sulfur elemental maps of S-CNT in F-CNT. As observed in Figure 2f, sulfur atoms are clearly incorporated into the carbon matrix. Raman spectroscopy was used to identify and quantitatively measure the defect density in the CNT materials. The spectra in Figure 2g shows

DOI: 10.1021/acssuschemeng.7b03580
ACS Sustainable Chem. Eng. 2018, 6, 93−98

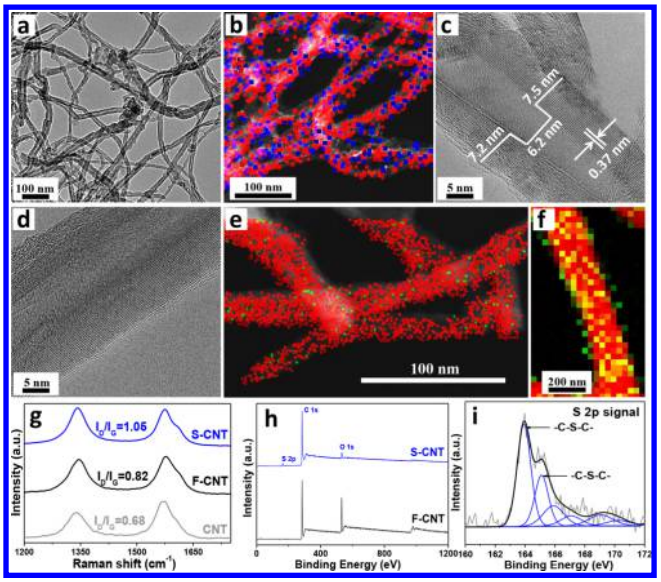

Figure 2. (a) SEM, (b) overlapping EDS maps of C (red) and O (blue); HRTEM of (c) F-CNT and (d) HRTEM, (e) overlapping EDS maps of C (red) and S (green); (f) EELS of S-CNT; (g) Raman spectra of CNT, F-CNT, and S-CNT; (h) full range XPS spectra of F-CNT and S-CNT; and (i) S 2p spectrum of S-CNT.

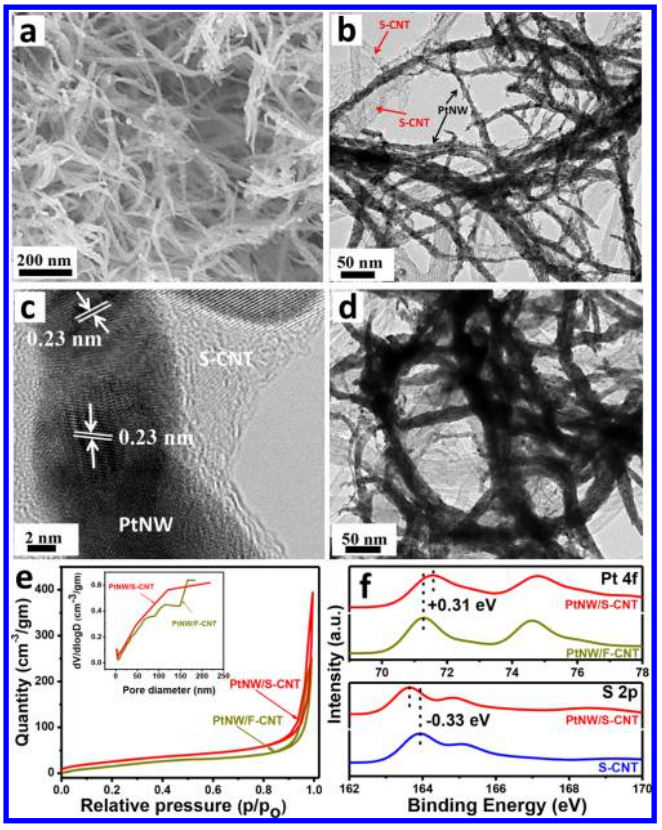

Figure 3. (a) SEM and (b) TEM images of PtNW/S-CNT; (c) HRTEM micrograph of Pt nanowire with 0.23 nm *d*-spacing corresponding to the (111) facet. (d) TEM image of PtNW/F-CNT. (e) N_2 sorption isotherm and pore size distribution (inset) in PtNW/S-CNT and PtNW/F-CNT. (f) Pt 4f spectra of PtNW/S-CNT and PtNW/F-CNT, and S 2p spectra of PtNW/S-CNT and S-CNT (note that, in panels b and d, the dark black is the PtNW and the light gray is the S-CNT).

that the ratios of D-band intensity to G-band intensity (I_D/I_G) are 0.68, 0.82, and 1.05 in CNT, F-CNT, and S-CNT, respectively. This result indicates that sulfur atoms are present in S-CNT as defects replacing carbon atoms via the reaction between PDS and oxygen-containing groups in F-CNT. Using XPS, the identity and concentration of the surface species on F-CNT and S-CNT were confirmed. Figure 2h displays the full range spectra of F-CNT and S-CNT, while their corresponding surface atomic concentrations are provided in Table S1. The XPS analysis was performed on S-CNT and the S 2p signal recorded at 161.1 eV revealed a surface concentration of 1.02 at. %. This indicates the effective incorporation of sulfur atoms onto the final CNT structure via the FHT method. Figure 2i shows high resolution XPS spectra of S 2p of S-CNT, which are deconvoluted into two major peaks positioned at 163.93 and 165.10 eV and four minor peaks located at energies above 165.92 eV. The two major peaks appears to develop from the S 2p spin−orbit doublet (S $2p_{1/2}$ and S $2p_{3/2}$, respectively) that can be associated with sulfur directly bonded to carbon atoms in the form of C−S−C.[21] It is likely that these C−S−C groups occur in the thiophene form, as supported by previously reported investigations and our formation energy calculations.[19] Furthermore, the pentagonal-structured thiophene species reside on the plane edge and defected sites of S-CNT and give rise to the appearance of the D band in the Raman spectra. The four minor peaks observed in the spectra can be associated with carbon bonded to SO_x species.[21]

Figure 3a,b shows scanning electron microscopy (SEM) and TEM images respectively, revealing the interconnected 3D architecture of PtNW/S-CNT. The nanowires have a diameter ranging from 4 to 28 nm, while their length exceeds 1 μm. Our previous investigation on the Pt nanowires growth on the surface of SG shows that the nanowires consist of numerous Pt nanoparticles linked together.[15] Similarly, according to the HR-TEM image in Figure 3c, the nanowires supported by S-CNT also appear to be composed of nanosized Pt particles joined together with a crystallographic allignment along the ⟨111⟩ direction and a distance of approximately 0.23 nm between (111) planes. Apart from our previous studies, we modified the synthesis and investigated the role of precursor materials in the formation of Pt nanowires in the presence of S-CNT (see Supporting Information for the experimental procedure, Figures S1−S7). The optimal conditions for obtaining the desired nanowire morphology is to use 15 mL of ethylene glycol, 15 mL of dimethylformamide (DMF), 1.5 g of KOH, 10 mg of Pt, and 10 mg of S-CNT during synthesis. This leads to growth of small-diameter Pt nanowires primarily in the range of 4−12 nm onto 1D nanostructured carbon supports such as S-CNT. However, the nanowires grown on undoped F-CNT tend to have larger diameters mostly in the range of 8−20 nm (Figure 3d and Figure S8). Sulfur in F-CNT appears to play a significant role in anchoring the direction of nanowire formation, binding the nanowires very tightly and thereby avoiding their agglomeration and detachment. BET analysis (Figure 3e) shows that PtNW/S-CNT possesses a specific surface area of 125 $m^2\ g^{-1}$, which is higher than that of PtNW/F-CNT (101 $m^2\ g^{-1}$). The pore size distribution clearly shows the presence of multiple porosities (micro/meso/macro) in the catalyst materials. It is interesting to note that PtNW/S-CNT is highly porous (total pore volume: 0.6 $cm^3\ g^{-1}$) and contains predominantly macropores (65%), whereas only 45% of the overall pore volume in PtNW/F-CNT (total pore volume: 0.38 $cm^3\ g^{-1}$) involves macropores. It has been reported that ORR

DOI: 10.1021/acssuschemeng.7b03580
ACS Sustainable Chem. Eng. 2018, 6, 93−98

performance can be improved with presence of macropores by reducing the diffusion length of reactive molecules.[22] Therefore, it is expected that the presence of numerous large pores should promote efficient electrocatalysis by PtNW/S-CNT. The Pt 4f spectra of PtNW/S-CNT and PtNW/CNT in Figure 3f (top) shows that both synthesized materials exhibit the characteristic zero-valence doublet of Pt with the Pt $4f_{7/2}$ and Pt $4f_{5/2}$ located at 71.56 and 75.80 eV in PtNW/S-CNT and 71.25 and 74.58 eV in PtNW/F-CNT. It was significant to note that the peak position in PtNW/S-CNT is shifted by 0.31 eV in the positive direction in comparison to that observed for PtNW/F-CNT, providing a clear indication of a strong interaction between Pt and S-CNT. Moreover, a noticeable negative peak shift in the S 2p peak for PtNW/S-CNT by 0.33 eV relative to that observed in S-CNT is observed (Figure 2f, bottom), indicating a transfer of electrons from S-CNT to Pt.

The cyclic voltammogram (CV) of PtNW/S-CNT immersed in N_2-saturated 0.1 M $HClO_4$ obtained at a sweeping rate of 50 mV s^{-1} is shown in Figure 4a. CV curves were obtained before and after cycling up to 3000 cycles between 0.05 and 1.5 V RHE to evaluate the long-term electrochemical stability of the catalysts. The hydrogen adsorption/desorption region was integrated between 0 and 0.4 V RHE to obtain electrochemocal active surface area (ECSA) and Q_{ref} = 0.21 mC cm^{-2} was taken for hydrogen monolayer adsorption.[18] The ECSA values obtained for PtNW/S-CNT before and after ADT were calculated to be 17.2 and 16.0 m^2 g^{-1}, respectively. For comparison, the stabilities of PtNW/F-CNT and commercial Pt/C catalyst (TKK, 28.2% Pt loading) were also evaluated (Figure S9). Under identical conditions, the ECSA values before and after ADT test were found to be 15.7 and 9.7 m^2 g^{-1}, respectively, for PtNW/F-CNT and 55.4 and 0.1 m^2 g^{-1}, respectively for Pt/C. Lowering of ECSA in PtNW/S-CNT and PtNW/F-CNT in comparison to Pt/C was expected due to the larger diameter and structural anisotropy of the nanowires that lowers the degree of Pt atom exposure.[6,7,23] Figure 4b shows typical ORR polarization curves of PtNW/S-CNT obtained at room temperature in O_2-saturated 0.1 M $HClO_4$, using rotating disc electrode (RDE) system at a rotation of 1600 rpm at a sweep rate of 5 mV s^{-1}. The electrochemical reduction reaches the mass transfer limit below 0.8 V RHE while the mixed kinetic-diffusion control region was observed between 0.8 and 1.0 V RHE. The polarization curves in Figure 4b obtained before and after ADT shows a loss of only 7 mV in the half-wave potential ($E_{1/2}$) for PtNW/S-CNT. At the same time, a loss of 54 mV in $E_{1/2}$ for PtNW/F-CNT and >400 mV loss for Pt/C were observed under identical conditions (Figure S10). The variation in normalized ECSA of the catalysts with the number of ADT cycles is plotted in Figure 4c. After 3000 cycles, PtNW/S-CNT, PtNW/F-CNT, and Pt/C lost 7%, 38%, and >99% of their initial ECSA, respectively. Clearly, these ADT results show that PtNW/S-CNT has a significantly higher stability after 3000 cycles and can withstand the harsh potentiodynamic conditions in fuel cells. We attribute this high durability of the stable stable structure of PtNW anchoring onto a network of S-CNT, where the sulfur atoms acting as anchoring sites. In our earlier investigation we showed that Pt has an affinity to adsorp strongly to sulfur sites in sulfur doped graphene. Similarly, we postulate this affinity will explaing the long durability of Pt-NWs/S-CNT as an electrocatalyst of ORR.

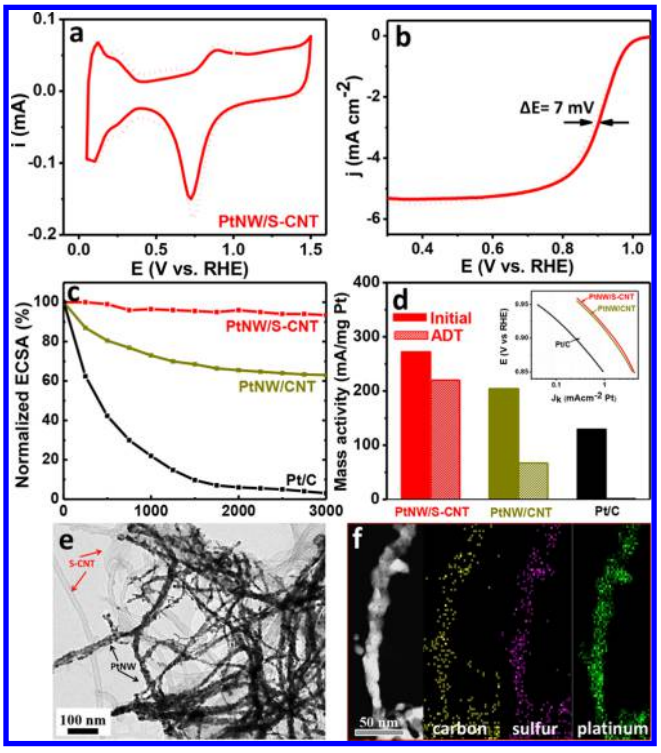

Figure 4. (a) Cyclic voltametry and (b) polarization curves of PtNW/S-CNT between 0.05 and 1.5 V vs RHE before and after 3000 potential cycles. (c) Effect of ADT cycle on normalized ECSA. (d) Bar chart plot of ORR mass activities of the synthesized catalysts at 0.9 V RHE before and after ADT; inset: Specific ORR activities of synthesized catalysts with Pt/C. (e) TEM image of PtNW/S-CNT after ADT (note that the dark black is the PtNW and the light gray is the S-CNT) and (f) elemental mapping showing the distribution of C (yellow), S (purple), and Pt (green) in PtNW/S-CNT.

The specific and mass activities are the most important parameters to indicate the performance of an electrocatalyst. As illustrated in Figure 4d (inset), PtNW/S-CNT achieves a specific activity of 1.61 mA $cm^{-2}{}_{Pt}$, which is better than that of PtNW/F-CNT (1.37 mA $cm^{-2}{}_{Pt}$) and Pt/C (0.244 mA $cm^{-2}{}_{Pt}$). A comparison of the Pt-based mass activities before and after ADT is also shown in Figure 4d. Prior to ADT, PtNW/S-CNT showed an improved mass activity of 272 mA $mg^{-1}{}_{Pt}$ in comparison with PtNW/F-CNT (204 mA $mg^{-1}{}_{Pt}$) and Pt/C (130 mA $mg^{-1}{}_{Pt}$). After the ADT, PtNW/S-CNT was able to retain a mass activity of 220 mA $mg^{-1}{}_{Pt}$, which is 81% of the initial value. On the other hand, the mass activities of PtNW/F-CNT and Pt/C dropped to 67 mA $mg^{-1}{}_{Pt}$ and 0.2 mA $mg^{-1}{}_{Pt}$ following the ADT, that is only 33% and <1% of their initial electrochemical activity before ADT, respectively. The improved stability and activity for the PtNW/S-CNT can be attributed to several factors: (1) 1D nature of S-CNT and Pt nanowires that facilitates easy mass/electron transport of reactants in the 3D architecture of PtNW/S-CNT; (2) fewer surface defects and preferential exposure of the (111) facets that exhibit higher specific activities; (3) interaction of chemically bonded sulfur species in F-CNT with Pt nanowires that leads to stronger attraction and binding of nanowires and increased stability. Additionally, the negative impacts on ORR resulted from strong bonding of adsorbed OH_{ad} species on the undesired sites (the defect, step and edge sites of nanoparticles) should be weakened by the 1D extended nanostructure of PtNWs.[24] The performance of the PtNWs electrocatalyst in this

DOI: 10.1021/acssuschemeng.7b03580
ACS Sustainable Chem. Eng. 2018, 6, 93−98

work has been compared with the results from literature in Table S2, in the Supporting Information.

The morphology of PtNW/S-CNT following the ADT was also investigated, and no visible morphology change was observed (Figure 4e). PtNWs were found to be attached on the S-CNT surface even after 3000 cycle. To further investigate, an energy dispersive spectroscopy (EDS) color mapping of PtNW/S-CNT is displayed in Figure 4f, which indicates that sulfur atoms are evenly dispersed along the length of the CNTs. Moreover, PtNWs tend to inhabit the regions that are rich in sulfur content, which reflects the affinity and strong binding between Pt nanowires and S-CNT. This clearly confirms the beneficial impact of S-CNT in hindering the dissolution, ripening, and aggregation of Pt nanowires, which would otherwise reduce both ORR activity and stability. In addition, the morphologies of PtNW/F-CNT and Pt/C were significantly affected by the harsh ADT conditions, leading to severe catalyst degradation and aggregation along with nanoparticle agglomeration (Figure S11).

In summary, a novel 1D S-CNT material has been prepared to support 1D Pt nanowires for ORR. The interconnected 3D nanoassemblies of Pt nanowires and S-CNT show a higher electrochemical activity and remarkable long-term stability in contrast to commercial Pt/C catalyst. After 3000 ADT cycles, PtNW/S-CNT still remains very stable and retains 93% of its initial ECSA, while PtNW/CNT and Pt/C retain only 62% and <1% of their initial ECSA, respectively. Additionally, the half-wave potential for PtNW/S-CNT decreases by only 7 mV, an exceptional improvement over PtNW/CNT and commercial Pt/C, which decreased by 54 mV and >400 mV, respectively. The Pt-based mass activity of PtNW/S-CNT was remarkable in comparison to PtNW/CNT and commercial Pt/C after ADT, showing outstanding durability. PtNW/S-CNT also exhibited an outstanding specific activity of 1.61 mA cm^{-2}_{Pt}, exceeding the DOE recommended target of 0.72 mA cm^{-2}_{Pt}. In view of these dramatic improvements in performance, S-CNT shows great promise as a new class of supports for PtNW ORR catalysts and could potentially replace conventional cathode catalysts in practical applications.

■ ASSOCIATED CONTENT

Supporting Information

The Supporting Information is available free of charge on the ACS Publications website at DOI: 10.1021/acssuschemeng.7b03580.

Experimental and synthesis details, additional SEM, TEM images, particle size distribution histograms, XPS surface concentration, and electrochemical results (PDF)

■ AUTHOR INFORMATION

Corresponding Author

*Z. Chen. E-mail: zhwchen@uwaterloo.ca.

ORCID

Siyu Ye: 0000-0002-4384-5025

Zhongwei Chen: 0000-0003-3463-5509

Author Contributions

[+]These authors contributed equally.

Notes

The authors declare no competing financial interest.

■ ACKNOWLEDGMENTS

This research was funded by the Natural Sciences and Engineering Research Council of Canada (NSERC). The authors thank Dr. Andrei Carmen, for TEM and EELS characterizations at the Canadian Center for Electron Microscopy (CCEM) at McMaster University.

■ REFERENCES

(1) Nie, Y.; Li, L.; Wei, Z. D. Recent advancements in Pt and Pt-free catalysts for oxygen reduction reaction. *Chem. Soc. Rev.* **2015**, *44* (8), 2168−2201.

(2) Peng, Z. M.; Yang, H. Synthesis and Oxygen Reduction Electrocatalytic Property of Pt-on-Pd Bimetallic Heteronanostructures. *J. Am. Chem. Soc.* **2009**, *131* (22), 7542−7543.

(3) Bing, Y. H.; Liu, H. S.; Zhang, L.; Ghosh, D.; Zhang, J. J. Nanostructured Pt-alloy electrocatalysts for PEM fuel cell oxygen reduction reaction. *Chem. Soc. Rev.* **2010**, *39* (6), 2184−2202.

(4) Xia, B. Y.; Ng, W. T.; Wu, H. B.; Wang, X.; Lou, X. W. Self-Supported Interconnected Pt Nanoassemblies as Highly Stable Electrocatalysts for Low-Temperature Fuel Cells. *Angew. Chem., Int. Ed.* **2012**, *51* (29), 7213−7216.

(5) Koenigsmann, C.; Zhou, W. P.; Adzic, R. R.; Sutter, E.; Wong, S. S. Size-Dependent Enhancement of Electrocatalytic Performance in Relatively Defect-Free, Processed Ultrathin Platinum Nanowires. *Nano Lett.* **2010**, *10* (8), 2806−2811.

(6) Sun, S. H.; Zhang, G. X.; Geng, D. S.; Chen, Y. G.; Li, R. Y.; Cai, M.; Sun, X. L. A Highly Durable Platinum Nanocatalyst for Proton Exchange Membrane Fuel Cells: Multiarmed Starlike Nanowire Single Crystal. *Angew. Chem., Int. Ed.* **2011**, *50* (2), 422−426.

(7) Liang, H. W.; Cao, X. A.; Zhou, F.; Cui, C. H.; Zhang, W. J.; Yu, S. H. A Free-Standing Pt-Nanowire Membrane as a Highly Stable Electrocatalyst for the Oxygen Reduction Reaction. *Adv. Mater.* **2011**, *23* (12), 1467−1471.

(8) Koenigsmann, C.; Santulli, A. C.; Gong, K. P.; Vukmirovic, M. B.; Zhou, W. P.; Sutter, E.; Wong, S. S.; Adzic, R. R. Enhanced Electrocatalytic Performance of Processed, Ultrathin, Supported Pd-Pt Core-Shell Nanowire Catalysts for the Oxygen Reduction Reaction. *J. Am. Chem. Soc.* **2011**, *133* (25), 9783−9795.

(9) Chen, Z. W.; Waje, M.; Li, W. Z.; Yan, Y. S. Supportless Pt and PtPd nanotubes as electrocatalysts for oxygen-reduction reactions. *Angew. Chem., Int. Ed.* **2007**, *46* (22), 4060−4063.

(10) Xia, B. Y.; Wu, H. B.; Yan, Y.; Lou, X. W.; Wang, X. Ultrathin and Ultralong Single-Crystal Platinum Nanowire Assemblies with Highly Stable Electrocatalytic Activity. *J. Am. Chem. Soc.* **2013**, *135* (25), 9480−9485.

(11) Liu, Y.; Li, D. G.; Sun, S. S. Pt-based composite nanoparticles for magnetic, catalytic, and biomedical applications. *J. Mater. Chem.* **2011**, *21* (34), 12579−12587.

(12) Guo, S. J.; Li, D. G.; Zhu, H. Y.; Zhang, S.; Markovic, N. M.; Stamenkovic, V. R.; Sun, S. H. FePt and CoPt Nanowires as Efficient Catalysts for the Oxygen Reduction Reaction. *Angew. Chem., Int. Ed.* **2013**, *52* (12), 3465−3468.

(13) Sun, S. H.; Jaouen, F.; Dodelet, J. P. Controlled Growth of Pt Nanowires on Carbon Nanospheres and Their Enhanced Performance as Electrocatalysts in PEM Fuel Cells. *Adv. Mater.* **2008**, *20* (20), 3900−3904.

(14) Sun, S. H.; Zhang, G. X.; Geng, D. S.; Chen, Y. G.; Banis, M. N.; Li, R. Y.; Cai, M.; Sun, X. L. Direct Growth of Single-Crystal Pt Nanowires on Sn@CNT Nanocable: 3D Electrodes for Highly Active Electrocatalysts. *Chem. - Eur. J.* **2010**, *16* (3), 829−835.

(15) Hoque, M. A.; Hassan, F. M.; Higgins, D.; Choi, J. Y.; Pritzker, M.; Knights, S.; Ye, S.; Chen, Z. Multigrain platinum nanowires consisting of oriented nanoparticles anchored on sulfur-doped graphene as a highly active and durable oxygen reduction electrocatalyst. *Adv. Mater.* **2015**, *27* (7), 1229−1234.

(16) Zhang, W. M.; Sherrell, P.; Minett, A. I.; Razal, J. M.; Chen, J. Carbon nanotube architectures as catalyst supports for proton

DOI: 10.1021/acssuschemeng.7b03580
ACS Sustainable Chem. Eng. 2018, 6, 93−98

exchange membrane fuel cells. *Energy Environ. Sci.* **2010**, *3* (9), 1286–1293.
(17) Chen, Y. G.; Wang, J. J.; Liu, H.; Li, R. Y.; Sun, X. L.; Ye, S. Y.; Knights, S. Enhanced stability of Pt electrocatalysts by nitrogen doping in CNTs for PEM fuel cells. *Electrochem. Commun.* **2009**, *11* (10), 2071–2076.
(18) Higgins, D. C.; Meza, D.; Chen, Z. W. Nitrogen-Doped Carbon Nanotubes as Platinum Catalyst Supports for Oxygen Reduction Reaction in Proton Exchange Membrane Fuel Cells. *J. Phys. Chem. C* **2010**, *114* (50), 21982–21988.
(19) Higgins, D.; Hoque, M. A.; Seo, M. H.; Wang, R.; Hassan, F.; Choi, J.-Y.; Pritzker, M.; Yu, A.; Zhang, J.; Chen, Z. Development and Simulation of Sulfur-doped Graphene Supported Platinum with Exemplary Stability and Activity Towards Oxygen Reduction. *Adv. Funct. Mater.* **2014**, *24* (27), 4325–4336.
(20) Wepasnick, K. A.; Smith, B. A.; Bitter, J. L.; Fairbrother, D. H. Chemical and structural characterization of carbon nanotube surfaces. *Anal. Bioanal. Chem.* **2010**, *396* (3), 1003–1014.
(21) Yang, Z.; Yao, Z.; Li, G. F.; Fang, G. Y.; Nie, H. G.; Liu, Z.; Zhou, X. M.; Chen, X.; Huang, S. M. Sulfur-Doped Graphene as an Efficient Metal-free Cathode Catalyst for Oxygen Reduction. *ACS Nano* **2012**, *6* (1), 205–211.
(22) Liang, J.; Zheng, Y.; Chen, J.; Liu, J.; Hulicova-Jurcakova, D.; Jaroniec, M.; Qiao, S. Z. Facile Oxygen Reduction on a Three-Dimensionally Ordered Macroporous Graphitic C3N4/Carbon Composite Electrocatalyst. *Angew. Chem., Int. Ed.* **2012**, *51* (16), 3892–3896.
(23) Ruan, L. Y.; Zhu, E. B.; Chen, Y.; Lin, Z. Y.; Huang, X. Q.; Duan, X. F.; Huang, Y. Biomimetic Synthesis of an Ultrathin Platinum Nanowire Network with a High Twin Density for Enhanced Electrocatalytic Activity and Durability. *Angew. Chem., Int. Ed.* **2013**, *52* (48), 12577–12581.
(24) Stamenkovic, V. R.; Fowler, B.; Mun, B. S.; Wang, G. F.; Ross, P. N.; Lucas, C. A.; Markovic, N. M. Improved oxygen reduction activity on Pt3Ni(111) via increased surface site availability. *Science* **2007**, *315* (5811), 493–497.

DOI: 10.1021/acssuschemeng.7b03580
ACS Sustainable Chem. Eng. 2018, 6, 93–98